

# Epicardial Fiber Organization in Swine Right Ventricle and Its Impact on Propagation

Frederick J. Vetter, Stephen B. Simons, Sergey Mironov, Christopher J. Hyatt, Arkady M. Pertsov

**Abstract**—Fiber organization is important for myocardial excitation and contraction. It can be a major factor in arrhythmogenesis and current distribution during defibrillation shocks. In this study, we report the discovery of a previously undetected thin epicardial layer in swine right ventricle (RV) with distinctly different fiber orientation, which significantly affects epicardial propagation. Experiments were conducted in isolated coronary-perfused right ventricular free wall preparations ( $n=8$ ) stained with the voltage-sensitive dye di-4-ANEPPS. Optical signals were recorded from the epicardium with a CCD video camera at 800 fps. Preparations were sectioned parallel to the epicardial surface with a resolution of 50  $\mu\text{m}$  or better. To link the histological data with the observed activation patterns, resulting fiber angles were introduced into a 3D computer model to simulate the electrical activation and voltage-dependent optical signals. In all preparations, we detected a thin epicardial layer with almost no depth-dependent fiber rotation. The thickness of this layer ( $z_0$ ) varied from 110 to 930  $\mu\text{m}$ . At the boundary of this layer, we observed an abrupt change in fiber angle by  $64 \pm 13^\circ$  followed by a gradual fiber rotation in the underlying layers. In preparations with  $z_0 < 700 \mu\text{m}$ , optical mapping during epicardial stimulation revealed unusual diamond- and rectangular-shaped activation fronts with two axes of fast conduction. Computer simulations accurately predicted the features of the experimentally recorded activation fronts. The free wall of swine RV has a thin epicardial layer with distinctly different fiber orientation, which can significantly affect propagation and give rise to unusually shaped activation fronts. This is important for understanding electrical propagation in the heart, and further refines the existing knowledge of myocardial fiber architecture. (*Circ Res.* 2005;96:244-251.)

**Key Words:** myofiber organization ■ optical mapping ■ propagation

The fiber organization of ventricular myocardium is a significant determinant of both its mechanical function and its electrical propagation<sup>1-3</sup>. Myocardial fiber organization has been implicated in the mechanisms of ventricular arrhythmias as one of the important factors responsible for the stability of 3D reentrant activity.<sup>4-8</sup> It is also thought to affect current distribution during defibrillation shocks<sup>9,10</sup> and thus affect their odds of failure and success. All this explains the persistent interest in structural aspects of myocardial organization<sup>11,12</sup> and motivates further refining the existing knowledge of myocardial fiber architecture.

The characteristic feature of myocardial fiber organization is the gradual counterclockwise rotation of fibers throughout the heart wall<sup>1,13-16</sup> with the total rotation angle from endocardium to epicardium across species ranging from 120° (dog) to 180° (pig).<sup>17,18</sup> Although in general the dependence of fiber rotation on depth is considered well established, information about fiber organization near the epicardial surface remains scarce.

There are indications in the literature<sup>15,19-21</sup> suggesting the existence in some species of a distinct epicardial layer that

breaks the pattern of gradual rotation and affects the epicardial<sup>20</sup> and transmural propagation.<sup>19</sup> An indirect indication in favor of such a layer was obtained in our recent optical mapping studies of the epicardial propagation in the pig RV free wall.<sup>20</sup> Instead of slightly distorted elliptical activation fronts, characteristic of anisotropic propagation in 3D tissue with gradual fiber rotation,<sup>22</sup> we observed diamond- and rectangular-shaped fronts with sharp corners. Propagation velocities along the diagonals of a rectangular front were close to 0.6 m/s, a characteristic conduction velocity along myocardial fibers in ventricular myocardium.<sup>23,24</sup>

These observations led us to hypothesize that the unusual activation patterns are caused by a yet uncharacterized thin epicardial layer with distinctly different fiber orientation. This layer does not follow the trend of gradual fiber rotation and significantly alters the pattern of the epicardial propagation.

The goal of this study was to test this hypothesis by carefully investigating the fiber organization in the epicardial layers and its effect on electrical propagation. We conducted extensive histological studies with improved spatial resolu-

Original received July 8, 2004; revision received November 9, 2004; accepted December 10, 2004.

From the Biomedical Engineering Program (F.J.V.), Department of Electrical and Computer Engineering, University of Rhode Island, Kingston; and Department of Pharmacology (S.B.S., S.M., C.J.H., A.M.P.), SUNY Upstate Medical University, Syracuse, NY.

Correspondence to Arkady M. Pertsov, PhD, Department of Pharmacology, SUNY Upstate Medical University, 750 E Adams St, Syracuse, NY 13210. E-mail pertsova@upstate.edu

© 2005 American Heart Association, Inc.

*Circulation Research* is available at <http://www.circresaha.org>

DOI: 10.1161/01.RES.0000153979.71859.e7

tion in which changes in fiber orientation were reconstructed as a function of wall depth. To achieve superior resolution near the epicardium compared with previous studies,<sup>16–18</sup> we collected serial sections at significantly smaller intervals (less than 50  $\mu\text{m}$ ). In addition, an automated algorithm was used to detect fiber orientation<sup>25</sup> and increase the accuracy of the fiber angle measurements.

To directly relate the histological data to the electrical activation patterns, we conducted optical mapping studies in all tissue samples before fixation and sectioning. To make the quantitative comparison between histological and optical mapping data, we introduced the experimentally derived fiber angles into 3D computer model to simulate optical signals on the epicardial surface of the heart. The simulation results were then compared with the optical mapping data obtained from the same preparation.

The main finding of our studies is the demonstration of previously undetected thin epicardial layer with fiber orientation significantly different from the underlying layers. We obtained compelling evidence from both computer simulations and optical mapping data that this layer has a major impact on epicardial propagation and gives rise to unusual diamond- and rectangular-shaped epicardial activation patterns. The introduction of the experimentally derived histological information into a computer model reproduced activation patterns that were fully consistent with the optical mapping data.

## Materials and Methods

### Isolated Coronary Perfused Swine RV Preparations

All experiments were performed in accordance with the *Guide for the Care and Use of Laboratory Animals* (NIH publication No. 85-23, revised 1996). Preparations were perfused with an oxygenated Tyrode solution at 37°C and 80 mm Hg and superfused with the same solution at a rate of 40 mL/min.<sup>26</sup> To the perfusate we added diacetyl-monoxime (DAM, 15 mmol/L) to inhibit contractions and the voltage-sensitive dye di-4-ANEPPS (15  $\mu\text{g}/\text{mL}$ ). The preparation was paced at a basic cycle length of 500 ms at twice the diastolic threshold within 10 mm of the center of the epicardial surface of the RV free. An expanded Materials and Methods section is presented in the online data supplement available at <http://circres.ahajournals.org>.

### Optical Data Acquisition and Signal Processing

The optical mapping apparatus consisted of a 12-bit digital CCD video camera (Dalsa CA-D1-0128T-STD). The area of interest ( $\approx 2.2 \times 2.2$  cm) was illuminated by a 250W tungsten halogen lamp. The fluorescence was excited at  $520 \pm 40$  nm and recorded at  $645 \pm 50$  nm. The images ( $64 \times 64$  pixels) were acquired at either 800 or 913 frames per second. Optical movies were postprocessed using custom routines written in PV-Wave (Visual Numerics Inc).

### Histological Analysis

After acquiring the optical mapping data, the preparation was perfused with 10% buffered formalin. A transmural block of tissue ( $\approx 1$  cm<sup>2</sup>) containing the stimulus site was then excised and photographed to record the original orientation and size of the sample for later reconstruction. The small block chosen for histological analysis was excised in the shape of asymmetric trapezoid that uniquely defined its orientation within the intact RV preparation. The center of the trapezoid corresponded to the stimulation site. The sample was then placed between two slices of cork to flatten the epicardial surface during fixation and paraffin embedding.

Serial sections (5 to 10  $\mu\text{m}$  thick) were cut parallel to the epicardial surface and stained with hematoxylin dye. Sections were imaged (261 pixels/mm) with a digital camera (SONY N50 progressive 3CCD). Several images ( $2.5 \times 1.3$  mm) were taken throughout each section to make sure that fiber direction was consistent. The mean fiber orientation in each image was calculated using an intensity gradient algorithm and circular statistics as described by Karlon et al.<sup>25</sup> Tissue shrinkage was measured in all sectioned samples. The measured degree of shrinkage was used to rescale the histological data and recover the actual depth of a given section before fixation.<sup>27</sup>

### Numerical Modeling

Electrical activity was simulated using the 3D cable equation:

$$(1) \quad \partial_t V_m = \nabla \cdot \tilde{D} \nabla V_m - I_{\text{ion}} / C_m,$$

where  $V_m$  is the transmembrane potential,  $C_m$  is membrane capacitance,  $I_{\text{ion}}$  is total ionic current density across the membrane, and  $\tilde{D}$  is the diffusion tensor reflecting the orientation of myocardial fibers inside the tissue. For the formulation of the ionic currents see our earlier publication.<sup>28</sup> The components of the diffusivity tensor  $\tilde{D}$  were calculated as described earlier.<sup>10,22</sup> The numerical values of the diffusion constants were  $D_L = 1$  cm<sup>2</sup>/s, and  $D_T = 1/9$  cm<sup>2</sup>/s, corresponding to electrical conduction velocity ratios of 10:3:3 in the longitudinal, transverse, and transmural directions, respectively.

The function  $\theta(z)$  that determines the depth dependence of the components of the diffusivity tensor  $\tilde{D}$  was derived from the measured fiber angles. In the epicardial layer (2 to 3 mm), it was approximated by a variation of the Boltzmann equation:

$$(2) \quad \theta(z) = \frac{A_2 - A_1}{1 + e^{(z - z_0)/d}} + A_1 + Bz,$$

where  $A_1$  is the fiber orientation after the transition,  $A_2$  is the fiber orientation at the epicardium, and  $B$  is the slope at the linear portions of the sigmoidal curve. The depth of the transition point is  $z_0$ , where the slope of  $\theta(z)$  is  $S_0 = (A_1 - A_2)/(4d)B$ . The parameter  $d$  scales the slope at the transition point. Linear fiber rotation was assumed for the remainder of the wall with the total transmural fiber rotation set to 180°.

Simulations were conducted on a  $3.2 \times 3.2 \times 0.8$  cm rectangular grid. No-flux boundary conditions were imposed at all boundaries.<sup>7</sup> Optical action potentials were computed in a  $2.2 \times 2.2$  cm region on the epicardial surface from the 3D distribution of the transmembrane voltage using the algorithm described previously.<sup>28</sup>

## Results

### Histological Analysis

Figure 1 shows the result of the histological analysis for one swine RV preparation. The top panel shows the profile of myocardial fiber angle versus wall depth. The fiber profile had a pronounced sigmoidal shape with almost no fiber rotation for depths less than 290  $\mu\text{m}$ . The fibers then abruptly rotated by approximately 63 degrees relative to the epicardial fibers at the top layer. The middle panel in Figure 1 shows the histological sections acquired at transmural depths of 75 and 550  $\mu\text{m}$ , demonstrating the abrupt change in fiber orientation across the transitional region. At locations deeper into the wall, the rotation continued but at a much slower rate. These data suggest the existence of a distinct epicardial layer with the thickness of approximately 290  $\mu\text{m}$ .

Similar results were obtained in other preparations. All of the transmural fiber profiles had a pronounced sigmoidal shape and were qualitatively similar to that shown in Figure 1. Yet, the depth of the transition from one fiber orientation to another, as well as its steepness, varied from preparation to

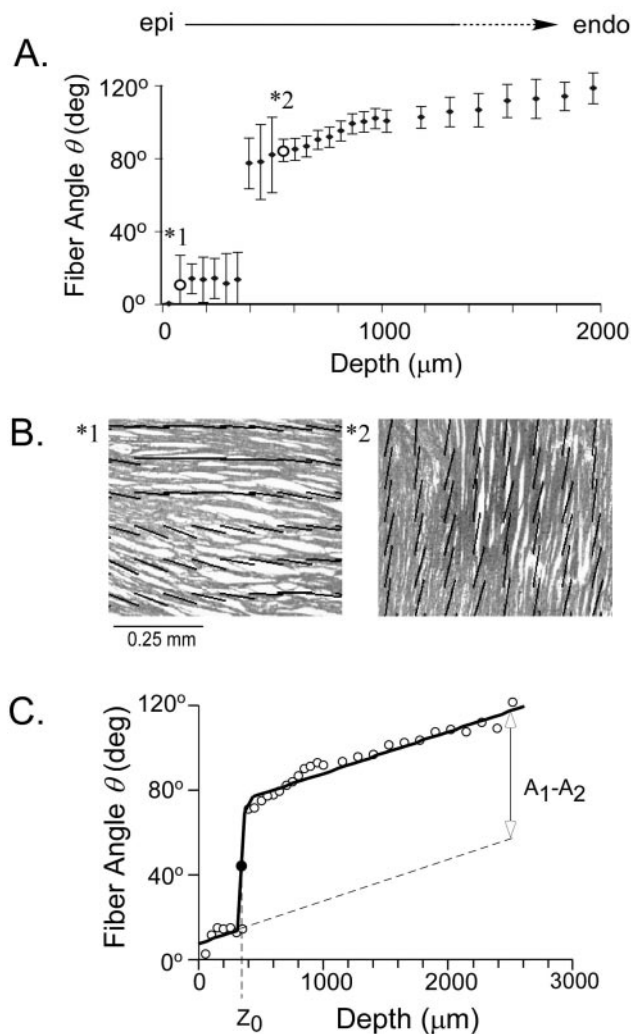


**Figure 1.** Abrupt change in local fiber orientation in swine RV subepicardium. A, Fiber angle as a function of depth, normalized to a zero angle at the epicardium. Abrupt change in fiber angle occurs at a depth of 291  $\mu\text{m}$ . Error bars show the standard deviation. B, Portions of two histological sections obtained at depths of 75  $\mu\text{m}$  (\*1) and 550  $\mu\text{m}$  (\*2). Solid lines show the local fiber orientation as determined by an automatic algorithm.<sup>25</sup> C, Fit of Equation 2 (solid line) to the measured fiber angles shown in A.

preparation. To quantify these variations, the fiber angles measured in each preparation were fit using Equation 2 (see Materials and Methods). Figure 1C shows the fit to the data presented in Figure 1A and illustrates the meaning of two major fitting parameters  $z_0$  and  $(A_1 - A_2)$ . Parameter  $z_0$  characterizes the thickness of the epicardial layer, whereas parameter  $(A_1 - A_2)$  indicates the change in fiber angle at the boundary of the epicardial layer.

Table 1 lists the numerical values of fitting parameters derived from the histological data for each of the eight preparations. The first two columns show the values of  $z_0$  and the magnitudes of change in fiber angle  $(A_1 - A_2)$ , respectively. In different preparations,  $z_0$  varied from 110 to 928  $\mu\text{m}$ , with the average being close to 500  $\mu\text{m}$ . The magnitude of  $(A_1 - A_2)$  showed less variability, although it had a tendency to decrease as  $z_0$  was located deeper into the wall.

The average magnitude of  $(A_1 - A_2)$  was approximately 64 degrees. The last two columns show the rates of fiber rotation inside ( $S_0$ ) and outside ( $B$ ) the transition region. The values of  $B$  were always significantly smaller than  $S_0$ . The values of  $S_0$  followed the same trend as  $(A_1 - A_2)$ : they tended to be smaller in preparations with larger  $z_0$ .

It should be noted that data presented in Table 1 reflect fiber organization only within the first 1.5 mm from the epicardial surface. Accordingly, values of parameter  $B$  do not represent the rate of fiber rotation in deep layers of the RV. The average rate of fiber rotation across the wall in these experiments was  $39 \pm 22$  degrees/mm, consistent with earlier histological studies.

### Fiber Organization and the Epicardial Activation Patterns

In all tissue samples before fixation and sectioning, we conducted optical mapping studies that enabled us to relate fiber organization to the epicardial activation patterns. Figure 2, top row, shows sequential snapshots of an expanding epicardial excitation front produced by epicardial point stimulation of the preparation whose fiber organization was illustrated in Figure 1. The first frame was recorded 6 ms after the stimulus, when the front had acquired a pronounced diamond shape with relatively sharp corners and two nearly perpendicular diagonals (dashed lines). The corners of the diamond remained relatively sharp and preserved their orientation as the wave expanded. Conduction velocity measured along the long diagonal (line 1 in Figure 2) was 0.61 m/s. Along the short diagonal (line 2), it was smaller (0.41 m/s). However, both velocities were within the range characteristic for propagation velocity along the longitudinal fiber direction.

To relate the activation pattern to the histological data shown in Figure 1, the fiber orientations were superimposed onto the images of the expanding excitation fronts. The dashed lines 1 and 2 in Figure 2 show the fiber orientation in the thin epicardial layer ( $z = 75 \mu\text{m}$ ) and in the underlying layer at  $z = 550 \mu\text{m}$ . Note that in the propagating wave, the orientation of the longer diagonal coincided with the surface fiber orientation, whereas the shorter diagonal was closely aligned with the fiber orientation deeper into the ventricular wall.

Similar correlation between the epicardial fiber organization and the shape of the excitation fronts was observed in other preparations. In 7 of 8 preparations, we observed diamond- and rectangular-shaped activation fronts with their diagonals aligned with the fiber orientation in the epicardial and the underlying layer respectively. (An example of a rectangular-shaped activation front is provided in Figure 3.) As can be seen in Table 2, the angle between diagonals derived from the optical mapping data were rather close to the values of  $(A_1 - A_2)$  characterizing the jump in fiber angle at the boundary of the thin epicardial layer and the underlying layers for the majority of the preparations.

As in the example described, in all experiments with diamond- and rectangular-shaped activation fronts, the average value of the conduction velocity along either of the diagonals was very close to the conduction velocity along

**TABLE 1. Characteristics of Fiber Organization in the Epicardium**

Experiment	Depth of Transition, $z_0$ , $\mu\text{m}$	Magnitude of Transition, $A_1-A_2$ , degrees	Slope at Transition, $S_0$ , degrees/mm	Slope at Plateaus, $B$ , degrees/mm
1	110	72	1281	81
2	291	73	3990	23
3	321	89	7194	17
4	525	63	278	45
5	556	56	137	17
6	584	58	201	16
7	689	50	393	23
8	928	52	118	23
Mean $\pm$ SD	501 $\pm$ 256	64 $\pm$ 13	1699 $\pm$ 2578	31 $\pm$ 22

Parameters derived from  $\theta(z)$  fitting using Equation 2.

myocardial fibers. Table 3 shows the ratios of conduction velocity along the diagonals. In all cases it was close to 1.

Comparison of histological and optical mapping data in different preparations suggests that the epicardial activation patterns are extremely sensitive to the thickness of the epicardial layer  $z_0$  and variations in the transmural fiber rotation,  $\theta(z)$ . Figure 3A shows three representative examples of various activation patterns in our experiments. The corresponding fiber profiles are illustrated in Figure 3B. Diamond-shaped activation patterns (left column) were observed in preparations with smaller  $z_0$  and largest  $A_1-A_2$  (profile 1 in Figure 3B). Similar patterns were also recorded in experiments 1 to 3 (see Table 1). Rectangular patterns (middle column) were associated with intermediate  $A_1-A_2$  values (profile 2); the classical ellipse pattern (experiment 8) was observed only at largest  $z_0$  and smallest  $A_1-A_2$  values (profile 3). The rectangular activation pattern was the most common, appearing in four of the eight experiments.

### Computer Modeling

Our next step was to confirm quantitatively the role of the fiber organization in the observed unusual shape of activation fronts. The histological data from four representative preparations were incorporated into the computer model to simulate the individual propagating wave fronts observed via optical mapping at the epicardial surface of these preparations.

The bottom row in Figure 2 shows an example of the simulated excitation front using the fitted fiber profile shown in Figure 1. The simulated wave front has a pronounced diamond shape similar to the actual front recorded in the same preparation (compare Figure 2, top row). The origin of the diamond shape can be qualitatively understood when considering a superposition of two conventional elliptical activation fronts, rotated with respect to each other. The first ellipse represents anisotropic propagation in the upper layer, whereas the second ellipse represents anisotropic propagation in the underlying layers (see Discussion for more detail).

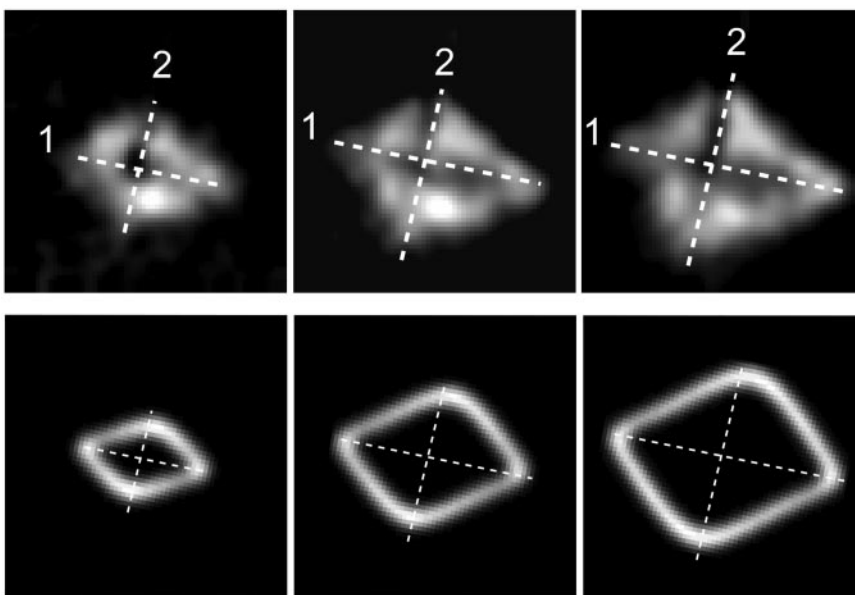


**Figure 2.** Experimental and simulated activation patterns on the epicardial surface. Top, Diamond-shaped epicardial activation pattern produced by point stimulation on the epicardial surface of swine RV. Images show the expanding wave front taken at 5 ms intervals from the time of stimulation. Dashed lines indicate the fiber orientation on the surface<sup>1</sup> and in the subsurface<sup>2</sup> layers (see histological sections in Figure 1). Bottom, Simulations of the epicardial excitation front at 5 ms intervals from the time of stimulation. Fiber orientation in the model was derived from the measured fiber angles. Diagonals show the axes of fast propagation and correspond to the epicardial surface and subsurface fiber orientations.

10 mm

Computer simulations also confirmed the sensitivity of epicardial activation patterns to the thickness of the epicardial layer and variations in the transmural fiber rotation,  $\theta(z)$ . Figure 3A shows examples of computed epicardial activation patterns in three different preparations. Simulations that used experimentally observed variations in the depth and slope of the transition point in the transmural fiber profiles were sufficient to produce dramatically different shapes (bottom row) of epicardial excitation fronts. In all cases, there was excellent agreement between the simulated and experimentally observed activation patterns.

### Discussion

The most important result of this study is the discovery of a thin epicardial layer in the RV of the pig with a distinctly different fiber orientation and its effect on propagation. We demonstrated that the abrupt fiber rotation occurring at the boundary of this layer produces unusual diamond and rectangular patterns of epicardial activation arising from point stimulation on the epicardial surface. We also showed that variations in the depth of the rapid fiber transition could cause dramatic differences in the shape of the epicardial activation pattern. Simulated activation patterns obtained using experimentally derived fiber angles showed excellent agreement with optical recordings. This provides further support to our histological findings and to our hypothesis that epicardial fiber organization is responsible for the unusual diamond-shaped and rectangular activation patterns observed during epicardial point stimulation.

### Nature of Unusually Shaped Activation Fronts

As mentioned, the origin of the diamond- and rectangular shapes of the activation fronts can be qualitatively understood when considering a superposition of two conventional elliptical activation fronts, rotated with respect to each other. The first ellipse represents anisotropic propagation in the top layer, whereas the second ellipse represents anisotropic propagation in the underlying layers. The major axis of each ellipse will coincide with the fiber orientation in its respective layer. For a large angle between the axes (80 degrees in our case), such a superposition gives rise to a diamond-like shape of the wave front at the epicardial surface. Indeed, the major axis of each ellipse forms the two diagonals of the diamond, whereas the minor axis of either ellipse is masked by major axis of the other, and cannot be observed.

The fact that the diagonals of the activation front approximately align with the fiber direction in the respective layer provides a simple explanation of rapid propagation along each of the diagonals in Figure 2. It is just a consequence of the fact that the propagation velocity along each of the diagonals represents the longitudinal conduction velocity.

The different length of diagonals (diamond shapes) in some experiments is likely attributable to the delay between the development of a detectable excitation front in the deeper and the top layers. (The stimulus applied at the epicardial surface activates the top layer first, giving rise to a larger ellipse.) The larger differences in the lengths of the diagonals may indicate reduced coupling between the top layer and the underlying layers postulated by Yan and coworkers.<sup>19</sup> It is

interesting that angles between diagonals derived from the optical mapping data were usually larger than the angles obtained by fitting histological data (the differences are shown in the last column of Table 2). These differences are likely a result of fiber rotation underneath the transition area. It is well established that epicardial optical mapping integrates signals originated from depths significantly exceeding 1 mm.<sup>28</sup> Accordingly, fibers located deep in the myocardial wall should contribute to the optical signal and thus increase the observed angle.

Another interesting issue is the variability of structural organization that we observed across specimens (Table 1). It is likely that the thickness of the outer layer, as well as the slope of the abrupt fiber transition, depends on its relative longitudinal position between the apex and base, and its proximity to papillary muscles and the intraventricular septum. A detailed analysis of factors that determine variability of structural organization of the epicardial layer in the pig RV should become a subject of future studies. It is worth noting that for successful prediction of the shape of the activation

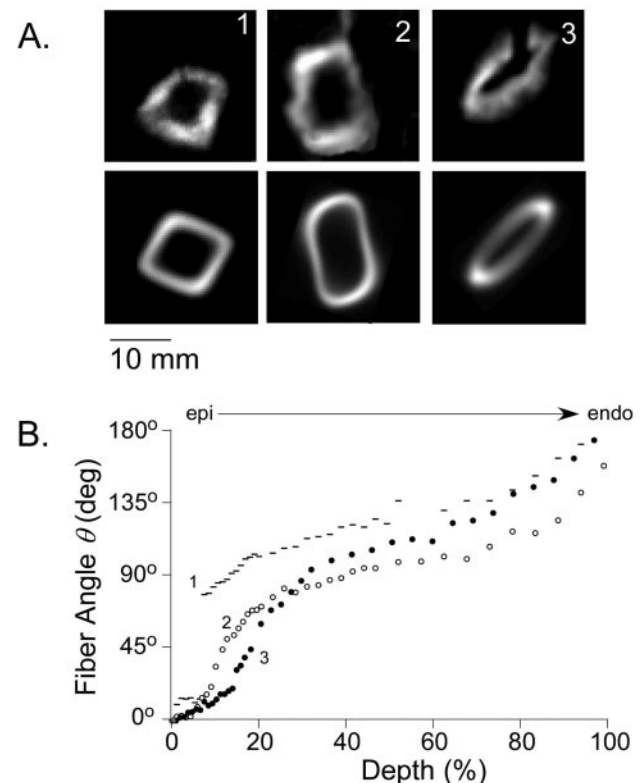


**Figure 3.** Epicardial activation patterns and transmural fiber orientation in three preparations. A, Epicardial wave fronts observed in the experimental preparations (top row) with the fiber profiles shown in the bottom panel. Numerical simulations (bottom row) with fiber profiles described by Equation 2 after fitting to the measured angles in the lower panel. All snapshots were taken 15 ms after stimulation. Columns 1, 2, and 3 correspond to the same-numbered fiber profiles shown in the bottom panel. B, Fiber profile 1 (dashed line, Experiment 2) showed the largest transition, which was nearest the epicardial surface. Transition point is deeper in fiber profile 2 (open circles, Experiment 5), and the slope is less steep. Fiber profile 3 (filled circles, Experiment 8) has the deepest transition point and flattest slope of the three curves.

**TABLE 2. Comparison Between Histological and Optical Mapping Data**

Experiment	Change in Fiber Direction,* $A_1 - A_2$	Angle Between Wave Front Diagonals*	Difference*
1	72	84	-12
2	73	90	-17
3	89	91	-2
4	63	65	-2
5	56	59	-3
6	58	67	-9
7	50	48	2
Mean±SD	66±13	72±17	-6.1±6.7

\*Degrees.

fronts, it was necessary to incorporate the unique histological data from the individual preparations into the numerical model. Using data averaged from all the tissue samples would likely not reproduce the unusual epicardial activation patterns that we observed experimentally. This emphasizes the need for precise structural descriptions to accurately predict the electrophysiological effects<sup>12</sup> in individual experimental preparations.

**Left Ventricle Versus Right Ventricle**

Analysis of the literature suggests that the left ventricle (LV) can exhibit a qualitatively similar sigmoidal pattern of fiber rotation that we observed in the RV. Figure 4 compares normalized profiles of fiber angle versus depth for the data we collected in the RV to the pig LV data reported by Streeter and Bassett.<sup>18</sup> Both plots were obtained by averaging data from several preparations, and appear qualitatively very similar: (1) both have an outer layer with almost no fiber rotation, (2) adjacent to the outer layer there is a region of rapid fiber rotation, (3) the rate of fiber rotation decreases toward midmyocardium and then increases again near the endocardium.

On an absolute scale, however, this means the epicardial layer is significantly wider in the LV than in the RV, and thus the maximal rate of fiber rotation in the LV is significantly less than in the RV. The electrophysiological implication of this geometric scaling is that diamond- or rectangular-shaped activation patterns on the surface of the LV are much less likely during epicardial point stimulation. This may explain, in part, why earlier optical mapping studies of the LV<sup>29</sup> have not reported similar observations.

**Generalization to Other Species**

The majority of existing histological studies provide little detail about the fiber orientation at shallow subepicardial depths.<sup>14,18</sup> However, there is evidence that a thin outer layer with a significantly different fiber orientation may exist in the

**TABLE 3. Ratio of Conduction Velocities Along the Main Axes in Experiments With Diamond-Shaped and Rectangular Activation Fronts**

Exp No.	1	2	3	4	5	6	7	Average
Ratio $V_1/V_2$	1.1	1.5	1.2	1	1.1	1.2	1.1	1.2±0.2

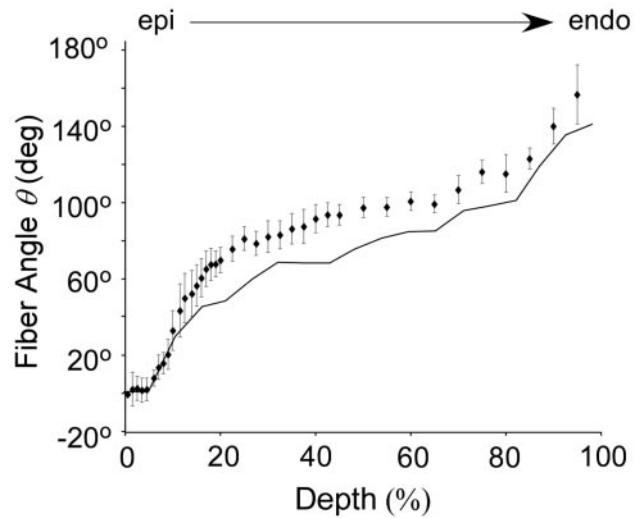


**Figure 4.** Transmural fiber angle profiles in swine RV and LV versus normalized wall depth. Points represent an average of all RV data described in this study. Solid line represents averaged data for the LV obtained by Streeter and Bassett.<sup>18</sup>

canine<sup>15,19</sup> and human<sup>21</sup> LV. In the human LV, Drouin et al<sup>21</sup> reported that the layers of epicardial cells are oriented perpendicular to the subepicardial layers, and hypothesized that the sharp transition was the transmural boundary between the epicardial cells and subepicardial cells (M cells). These studies suggest that the existence of an epicardial layer with distinctly different fiber orientation is not unique to the pig RV and is likely to be present in other species.

**Implications for Arrhythmogenesis and Defibrillation**

The epicardial layer with distinctly different fiber orientation in certain conditions may partially decouple from the rest of the myocardium and become arrhythmogenic. The findings of Drouin et al<sup>21</sup> in the human LV in which such a layer has been detected, show a sharp transition in action potential duration across the layer boundary. This led them to speculate that the electrical coupling between the layers is poor. In the canine LV, Yan et al<sup>19</sup> showed that tissue resistivity rose sharply at the subepicardium, where they identified an abrupt shift in fiber orientation that led them to arrive to a similar conclusion. Although normally in our experiments we did not observe any indications of electrical uncoupling between the epicardial layer and underlying layers, we did observe a significant degree of electrical uncoupling and reentry during acute global ischemia. The result of one such experiment in the ischemic pig RV is presented in the online data supplement. It shows how the ischemia-induced decoupling allowed the wave propagating in the deeper layer to become reentrant in the thin epicardial layer.

The abrupt fiber rotation attributable to the epicardial layer may affect not only the initiation but also the dynamics of 3D reentry. It has been demonstrated computationally that rapid fiber rotation can affect the shape of 3D reentrant activity<sup>5</sup> and may cause its transition to fibrillation.<sup>4</sup> The organization of myocardial fibers can also affect the distribution of

so-called “virtual electrodes” during electrical defibrillation, which may determine the outcome of the procedure.<sup>30,31</sup> It would be interesting to revisit these simulations in light of our findings.

### Limitations

The rapid fiber rotation could significantly complicate accurate measurements of the fiber angle in subsurface layers. Accurate measurements require the histological sections to be precisely aligned with the epicardial surface, which we achieved by flattening the epicardial preparations before fixation and careful specimen alignment on the microtome. The precision of alignment was the most critical when the steepness of the transition was very high. Misalignment, however, could be readily identified in transitional sections by the presence of patches with significantly different fiber angles and such sections were excluded from our analysis. This limited the depth resolution of our histological analysis to  $\approx 50 \mu\text{m}$ , yet this resolution is still superior to earlier histological studies.

The limited depth resolution might have affected the accuracy of fitting the maximal slope of the function  $\theta(z)$  and, in part, was likely responsible for its variability. This limitation, however, was a factor only in experiments with the maximal slopes (see Table 1, Experiments 1 to 3). In experiments 4 to 7, where the depth of the transition was deeper and the slope at the transition was less, we did not observe significant variations in fiber angle in transitional sections that would suggest any misalignment. In each of these experiments, we obtained multiple sections from the transitional area, which enabled us to measure the slope with a high degree of confidence.

The histological sections were always smaller than the area of the optically mapped epicardium. We are confident, however, that the epicardial fiber orientation was relatively constant across the mapped surface for two reasons. First, the relative uniformity of fiber orientation on the central RV epicardial surface has been suggested by the fiber reconstructions in the heart of the dog,<sup>14</sup> rabbit,<sup>32</sup> and most recently the pig.<sup>33</sup> Second, we did not detect a change in the direction of fast conduction along the long (epicardial) diagonal in any of the mapped preparations, suggesting that the fiber orientation was uniform on the mapped surface.

For modeling the electrical propagation, we used a monodomain formulation with a simplified description of ionic currents.<sup>4</sup> We also did not account for the laminar myocardial structure that may affect the properties of the diffusivity tensor.<sup>34</sup> Despite these simplifying assumptions, the simulation results accurately predicted the observed shapes of the epicardial excitation front. This suggests that subsurface fiber direction is a major factor affecting the geometry of the surface excitation fronts during epicardial point stimulation.

### Acknowledgments

This work was supported by NIH grant P20-RR016457 from the BRIN program of the National Center for Research Resources (to F.J.V.), as well as by grants from the National Heart, Lung and Blood Institute: 1R01-HL071635–01, 2PO1-HL39707 (to A.M.P., S.F.M., S.B.S.). Computational resources for the 3D simulations were

provided by the University of Rhode Island Department of Electrical & Computer Engineering.

### References

1. Streeter DD. Gross morphology and fiber geometry of the heart. In: Robert M. Berne, ed. *Handbook of Physiology, Section 2: The Cardiovascular System*. Bethesda, Md: American Physiological Society; 1979.
2. Taccardi B, Macchi E, Lux RL, Ershler PR, Spaggiari S, Baruffi S, Vyhmeister Y. Effect of myocardial fiber direction on epicardial potentials. *Circulation* 1994;90:3076–3090.
3. Roberts DE, Hersh LT, Scher AM. Influence of cardiac fiber orientation on wavefront voltage, conduction velocity, and tissue resistivity in the dog. *Circ Res* 1979;44:701–712.
4. Fenton F, Karma A. Vortex dynamics in three-dimensional continuous myocardium with fiber rotation: Filament instability and fibrillation. *Chaos* 1998;8:20–47.
5. Panfilov AV, Keener JP. Generation of reentry in anisotropic myocardium. *J Cardiovasc Electrophysiol* 1993;4:412–421.
6. Wellner M, Berenfeld O, Pertsov AM. Predicting filament drift in twisted anisotropy. *Phys Rev E Stat Phys Plasmas Fluids Relat Interdiscip Topics* 2000;61:1845–1850.
7. Berenfeld O, Pertsov AM. Dynamics of intramural scroll waves in three-dimensional continuous myocardium with rotational anisotropy. *J Theor Biol* 1999;199:383–394.
8. Wellner M, Berenfeld O, Jalife J, Pertsov AM. Minimal principle for rotor filaments. *Proc Natl Acad Sci U S A* 2002;99:8015–8018.
9. Knisley SB, Trayanova N, Aguel F. Roles of electric field and fiber structure in cardiac electric stimulation. *Biophys J* 1999;77:1404–1417.
10. Trayanova N, Skoubine K. Modeling defibrillation: effects of fiber curvature. *J Electrocardiol* 1998;31:23–29.
11. Scollan DF, Holmes A, Zhang J, Winslow RL. Reconstruction of cardiac ventricular geometry and fiber orientation using magnetic resonance imaging. *Ann Biomed Eng* 2000;28:934–944.
12. Muzikant AL, Hsu EW, Wolf PD, Henriquez CS. Region specific modeling of cardiac muscle: comparison of simulated and experimental potentials. *Ann Biomed Eng* 2002;30:867–883.
13. Torrent-Guasp F. *The Cardiac Muscle*. Madrid: Juan March Foundation; 1973.
14. Nielsen PM, Le Grice IJ, Smail BH, Hunter PJ. Mathematical model of geometry and fibrous structure of the heart. *Am J Physiol* 1991;260:H1365–H1378.
15. Thomas CE. The muscular architecture of the ventricles of hog and dog hearts. *Am J Anatomy* 1957;101:17–57.
16. Armour JA, Randall WC. Structural basis for cardiac function. *Am J Physiol* 1970;218:1517–1523.
17. Streeter DD Jr., Spotnitz HM, Patel DP, Ross J Jr, Sonnenblick EH. Fiber orientation in the canine left ventricle during diastole and systole. *Circ Res* 1969;24:339–347.
18. Streeter D.D. Jr., Bassett D. L. An Engineering Analysis of Myocardial Fiber Orientation in Pig's Left Ventricle in Systole. *Anat Rec* 1966;155:503–511.
19. Yan GX, Shimizu W, Antzelevitch C. Characteristics and distribution of M cells in arterially perfused canine left ventricular wedge preparations. *Circulation* 1998;98:1921–1927.
20. Simons SB, Vetter F, Mironov S, Hyatt C, Pertsov AM. Non-uniform fiber rotation in swine RV subepicardium and its implications for electrical conduction. *Proc Physiol Soc Uni Leeds* 10:55P.
21. Drouin E, Charpentier F, Gauthier C, Laurent K, Le Marec H. Electrophysiologic characteristics of cells spanning the left ventricular wall of human heart: evidence for presence of M cells. *J Am Coll Cardiol* 1995;26:185–192.
22. Franzone PC, Guerri L, Pennacchio M, Taccardi B. Spread of excitation in 3-D models of the anisotropic cardiac tissue, II: effects of fiber architecture and ventricular geometry. *Math Biosci* 1998;147:131–171.
23. Kleber AG, Janse MJ, Wilms-Schopmann FJ, Wilde AA, Coronel R. Changes in conduction velocity during acute ischemia in ventricular myocardium of the isolated porcine heart. *Circulation* 1986;73:189–198.
24. Hiraoka M, Hirano Y. Changes in passive electrical properties of guinea-pig ventricular muscle exposed to low  $K^+$  and high  $Ca^{2+}$  conditions. *J Mol Cell Cardiol* 1986;18:1177–1186.

25. Karlon WJ, Covell JW, McCulloch AD, Hunter JJ, Omens JH. Automated measurement of myofiber disarray in transgenic mice with ventricular expression of ras. *Anat Rec* 1998;252:612–625.
26. Zaitsev AV, Berenfeld O, Mironov SF, Jalife J, Pertsov AM. Distribution of excitation frequencies on the epicardial and endocardial surfaces of fibrillating ventricular wall of the sheep heart. *Circ Res* 2000;86:408–417.
27. Hsu EW, Muzikant AL, Matulevicius SA, Penland RC, Henriquez CS. Magnetic resonance myocardial fiber-orientation mapping with direct histological correlation. *Am J Physiol* 1998;274:H1627–H1634.
28. Hyatt CJ, Mironov SF, Wellner M, Berenfeld O, Popp AK, Weitz DA, Jalife J, Pertsov AM. Synthesis of voltage-sensitive fluorescence signals from three-dimensional myocardial activation patterns. *Biophys J* 2003;85:2673–2683.
29. Efimov IR, Ermentrout B, Huang DT, Salama G. Activation and repolarization patterns are governed by different structural characteristics of ventricular myocardium: experimental study with voltage-sensitive dyes and numerical simulations. *J Cardiovasc Electrophysiol* 1996;7:512–530.
30. Hooks DA, Tomlinson KA, Marsden SG, LeGrice IJ, Smaill BH, Pullan AJ, Hunter PJ. Cardiac microstructure: implications for electrical propagation and defibrillation in the heart. *Circ Res* 2002;91:331–338.
31. Trayanova N, Skouibine K, Aguel F. The role of cardiac tissue structure in defibrillation. *Chaos* 1998;8:221–233.
32. Vetter FJ, McCulloch AD. Three-dimensional analysis of regional cardiac function: a model of rabbit ventricular anatomy. *Prog Biophys Mol Biol* 1998;69:157–183.
33. Stevens C, Remme E, LeGrice I, Hunter P. Ventricular mechanics in diastole: material parameter sensitivity. *J Biomech* 2003;36:737–748.
34. LeGrice IJ, Smaill BH, Chai LZ, Edgar SG, Gavin JB, Hunter PJ. Laminar structure of the heart: ventricular myocyte arrangement and connective tissue architecture in the dog. *Am J Physiol* 1995;269:H571–H582.